

THE RELATIONSHIP BETWEEN GALAXY ISM AND CIRCUMGALACTIC GAS METALLICITIES

GLENN G. KACPRZAK¹, STEPHANIE K. POINTON^{1,2}, NIKOLE M. NIELSEN¹, CHRISTOPHER W. CHURCHILL³, SOWGAT MUZAHID², JANE C. CHARLTON⁴

ABSTRACT

We present ISM and CGM metallicities for 25 absorption systems associated with isolated star-forming galaxies ($\langle z \rangle = 0.28$) with $9.4 \leq \log(M_*/M_\odot) \leq 10.9$ and with absorption detected within 200 kpc. Galaxy ISM metallicities were measured using $H\alpha/[NII]$ emission lines from Keck/ESI spectra. CGM single-phase low-ionization metallicities were modeled using MCMC and Cloudy analysis of absorption from *HST*/COS and Keck/HIRES or VLT/UVES quasar spectra. We find that the star-forming galaxy ISM metallicities follow the observed stellar mass metallicity relation (1σ scatter 0.19 dex). CGM metallicity shows no dependence with stellar mass and exhibits a scatter of ~ 2 dex. All CGM metallicities are lower than the galaxy ISM metallicities and are offset by $\log(dZ) = -1.17 \pm 0.11$. There is no obvious metallicity gradient as a function of impact parameter or virial radius ($< 2.3\sigma$ significance). There is no relationship between the relative CGM–galaxy metallicity and azimuthal angle. We find the mean metallicity differences along the major and minor axes are -1.13 ± 0.18 and -1.23 ± 0.11 , respectively. Regardless of whether we examine our sample by low/high inclination or low/high impact parameter, or low/high $N(HI)$, we do not find any significant relationship with relative CGM–galaxy metallicity and azimuthal angle. We find that 10/15 low column density systems ($\log N(HI) < 17.2$) reside along the galaxy major axis while high column density systems ($\log N(HI) \geq 17.2$) reside along the minor axis. This suggests $N(HI)$ could be a useful indicator of accretion/outflows. We conclude that CGM is not well mixed, given the range of galaxy-CGM metallicities, and that metallicity at low redshift might not be a good tracer of CGM processes. On the other-hand, we should replace integrated line-of-sight, single phase, metallicities with multi-phase, cloud-cloud metallicities, which could be more indicative of the physical processes within the CGM.

Subject headings: galaxies: halos — quasars: absorption lines

1. INTRODUCTION

It is undeniable that there exists a massive reservoir of multi-phase gas that resides around star-forming galaxies (Tumlinson et al. 2017). A large collection of works provide evidence that outflows and accretion are ongoing processes that continuously change the properties of the circumgalactic medium (CGM) and the host galaxies. Low ionization level ions within the CGM show strong kinematic signatures that are consistent with large-scale outflows (Bouché et al. 2006; Tremonti et al. 2007; Martin & Bouché 2009; Weiner et al. 2009; Nestor et al. 2011; Noterdaeme et al. 2010; Coil et al. 2011; Kacprzak et al. 2010; Kacprzak et al. 2014; Rubin et al. 2010; Ménard & Fukugita 2012; Martin et al. 2012; Noterdaeme et al. 2012; Krogager et al. 2013; Péroux et al. 2013; Rubin et al. 2014; Crighton et al. 2015; Nielsen et al. 2015, 2016; Lan & Mo 2018). Furthermore, low angular momentum and co-rotating gas around galaxies and orientation dependent absorption velocity widths point to signatures of gas accretion (Steidel et al. 2002; Kacprzak et al. 2010; Ho et al. 2017; Kacprzak 2017; Martin et al. 2019; Zabl et al. 2019).

The CGM, as traced by Mg II absorption, appears to have a preference to exist along the major and minor axes of galaxies (Bouché et al. 2012; Kacprzak et al. 2012a; Schroetter et al. 2019), while the equivalent width of the absorption is highest

along the galaxy minor axis (Bordoloi et al. 2011; Kacprzak et al. 2012a; Lan et al. 2014; Lan & Mo 2018). This geometric dependence could be additional evidence for outflows and accretion. Furthermore, the metallicity distribution bimodality found for $z < 0.4$ Lyman limit systems (LLS) and partial Lyman limit systems (pLLS) shows a high ($[X/H] \sim -0.4$) and a low ($[X/H] \sim -1.7$) metallicity peak that could be attributed to being caused by outflows and accretion (Lehner et al. 2013, 2019; Wotta et al. 2016, 2019). Thus the spatial distribution of metallicity around galaxies would seem to be a likely key to understanding the origins of the CGM.

Numerous studies have obtained the CGM metallicity associated with a known galaxy in an effort to determine the origin and history of the absorption. These CGM metallicities generally reflect the metallicity bimodality where systems near galaxies are either metal-poor with metallicities between $-2 < [X/H] < -1$ (Tripp et al. 2005; Cooksey et al. 2008; Kacprzak et al. 2010b; Ribaldo et al. 2011; Thom et al. 2011; Churchill et al. 2012; Bouché et al. 2013; Crighton et al. 2013a; Stocke et al. 2013; Kacprzak et al. 2014; Crighton et al. 2015; Muzahid et al. 2015; Bouché et al. 2016; Fumagalli et al. 2016; Péroux et al. 2016) or metal-enriched with metallicities of $[X/H] > -0.5$ (Chen et al. 2005; Péroux et al. 2011; Krogager et al. 2013; Stocke et al. 2013; Crighton et al. 2015; Muzahid et al. 2015, 2016; Péroux et al. 2016). However, little is known about the host galaxy geometry with respect to the quasar sight-line in most cases. Using a sample of 47 galaxies with measured morphologies/orientations and CGM metallicities, Pointon et al. (2019a) has shown that CGM metallicities do not correlate with azimuthal angle or inclination of the galaxy regardless of impact parameter and $N(HI)$. Thus, it is possible that the spatial azimuthal depen-

¹ Swinburne University of Technology, Victoria 3122, Australia
gkacprzak@swin.edu.au

² ARC Centre of Excellence for All Sky Astrophysics in 3 Dimensions (ASTRO 3D)

³ Leiden Observatory, Leiden University, P.O. Box 9513, 2300 RA Leiden, The Netherlands

⁴ New Mexico State University, Las Cruces, NM 88003, USA

⁵ The Pennsylvania State University, State College, PA 16801, USA

dence and the metallicity bimodality are unrelated.

However, we do not fully understand how the host galaxy-ISM metallicities relate to the CGM metallicities. Since CGM galaxies span a range of stellar mass and given that there is a well-known galaxy stellar mass and ISM metallicity relation found at all redshifts (e.g. Tremonti et al. 2004; Sanders et al. 2014; Steidel et al. 2014; Zahid et al. 2014; Kacprzak et al. 2015b), then it is possible that the difference between the ISM and CGM metallicities would be more telling of the origins of the CGM.

Initial work from Prochaska et al. (2017) has shown that for ~ 20 systems, the CGM metallicity does not correlate with the ISM metallicity of host galaxies. In addition, work by Péroux et al. (2016) examined the metallicity difference between the galaxy ISM metallicity and CGM metallicity for nine systems. They found at low azimuthal angles, there are a range of ISM-CGM metallicity differences which would be unexpected for accreting gas. They only had two lower ISM-CGM metallicity systems along the minor axis, which is also unexpected for an outflow model. Fully exploring the relative galaxy ISM-CGM metallicities could provide additional insight into the relationship between galaxies and ongoing processes within the CGM.

We aim to further explore the relationship between the galaxy ISM and CGM metallicities and how they relate to the expectations of accretion/outflow models. We have acquired Keck/ESI spectra for 25 star-forming galaxies to obtain their ISM metallicities and their CGM metallicities are derived in Pointon et al. (2019a). We examine the stellar mass-metallicity relation for the galaxies and the CGM and test if the relative metallicity difference, defined to be the difference between the ISM and CGM metallicities, is dependent on hydrogen column density and/or galaxy properties such as azimuthal angle, inclination angle, and impact parameter. In Section 2 we present our sample, data and data reduction. In Section 3 we present our observational results. In Section 4, we discuss what can be inferred from the results and concluding remarks are offered in Section 5. Throughout we adopt an $H_0 = 70 \text{ km s}^{-1} \text{ Mpc}^{-1}$, $\Omega_M = 0.3$, $\Omega_\Lambda = 0.7$ cosmology.

2. SAMPLE AND DATA ANALYSIS

We have obtained galaxy ISM and CGM metallicities for 25 of the 47 systems selected from Pointon et al. (2019a), having a redshift range of $0.07 < z < 0.50$ within $\sim 200 \text{ kpc}$ ($21 < D < 203 \text{ kpc}$) of background quasars. The Pointon et al. (2019a) absorption systems were selected based on the presence of hydrogen having a column density range of $\log(N(\text{H I})) = 14 - 20$ and did not require the presence, but must have existing spectral coverage, of metal-lines. Our subset of 25 galaxies were selected to be star-forming such that we are able to obtain emission-line metallicities from Keck/ESI spectra. Pointon et al. (2019a) selected galaxies that are isolated such that there are no other galaxies within 100 kpc and with velocity separations less than 500 km s^{-1} . From our survey, and in the literature, the quasars fields have been surveyed to the equivalent of a sensitivity of $\geq 0.1 L_*$ out to at least 350 kpc at $z = 0.2$. These *HST* imaged galaxy-absorber systems were identified as part of our ‘‘Multiphase Galaxy Halos’’ Survey [from PID 13398 (Kacprzak et al. 2015a, 2018; Muzahid et al. 2015, 2016; Nielsen et al. 2017; Pointon et al. 2017, 2019a; Ng et al. 2019) and from the literature (Chen et al. 2001; Chen & Mulchaey 2009; Prochaska et al. 2011; Werk et al. 2012, 2013; Johnson et al. 2013)]. We discuss the

data and analysis below.

2.1. Quasar Spectroscopy and Models

The *HST/COS* quasar spectra have a resolution of $R \sim 20,000$ and cover a range of hydrogen and metal absorption lines associated with the targeted galaxies. Details of the *HST/COS* observations are found in Kacprzak et al. (2015a) and Pointon et al. (2019a). The data were reduced using the CALCOS software. Individual grating integrations were aligned and co-added using the IDL code ‘coadd_x1d’ created by Danforth et al. (2010)⁶. Since the COS FUV spectra are over-sampled, we binned the spectra by three pixels to increase the signal-to-noise and all of our analysis was performed on the binned spectra. Continuum normalization was performed by fitting the absorption-free regions with smooth low-order polynomials.

We further use Keck/HIRES or VLT/UVES quasar spectra when available to complement our COS spectra by including coverage of Mg I, Mg II, Fe II, Mn II and Ca II absorption, which provide additional metallicity constraints for absorbers with $z_{\text{abs}} > 0.2$. HIRES spectra were reduced using either the Mauna Kea Echelle Extraction (MAKEE) package or IRAF. The UVES spectra were reduced using the European Southern Observatory (ESO) pipeline (Dekker et al. 2000) and the UVES Post- Pipeline Echelle Reduction (UVES POPLER) software (Murphy et al. 2019).

We adopted the CGM metallicities modeled from Pointon et al. (2019a). In summary, the CGM metallicities were modeled using a combination of either *HST/COS* or *HST/COS*+Keck/HIRES or VLT/UVES spectra. The column densities were obtained from Voigt profile fits modeled using VPFIT (Carswell & Webb 2014). Pointon et al. (2019a) account for a non-Gaussian line spread function (LSF) of the COS spectrograph by using its wavelength dependant LSF (Kris 2011) convolved with the model profile during the fitting process. They assumed Gaussian LSF for the HIRES and UVES data. When fitting the absorption profiles, they fit the minimum number of components to obtain a satisfactory fit with reduced $\chi^2 \sim 1$.

The CGM metallicities are calculated in Pointon et al. (2019a) by fitting a grid of ionization properties generated by the ionization modeling suite Cloudy to the calculated column densities (Ferland et al. 2013). We assume a uniform single-phase layer of gas, with no dust, having solar abundance that is irradiated by a background UV spectrum. We adopt the HM05 UV background to generate the grids to be consistent with previous surveys (Lehner et al. 2013; ?; Wotta et al. 2016, 2019). We used the Markov Chain Monte Carlo (MCMC) technique described by Crighton et al. (2013a) to find the best-fit metallicity (quoted as the [Si/H] ratio) and ionization parameter to the measured column densities. The modeled $N(\text{H I})$ and CGM metallicities adopted from Pointon et al. (2019a) are shown in Table 1.

2.2. HST Imaging and Galaxy Models

All galaxy inclination angles and galaxy-quasar azimuthal angles were adopted from Kacprzak et al. (2015a) and Pointon et al. (2019a). All quasar/galaxy fields have been imaged with *HST* using either ACS, WFC3 or WFPC2. Details of the observations are found in Kacprzak et al. (2015a). ACS and WFC3 data were reduced using the DrizzlePac software

⁶ <http://casa.colorado.edu/danforth/science/cos/costools.html>

TABLE 1
 ABSORPTION AND HOST GALAXY PROPERTIES

Quasar ^a field	z_{gal}^b	M_r (AB)	R_{vir} (kpc)	$\log(M_h)$ (M_{\odot})	$\log(M_*)$ (M_{\odot})	$\log(\text{O}/\text{H})+12^b$	i (degree)	Φ (degree)	D (kpc)	$\log N(\text{H I})$ Measured (cm^{-2})	$\log N(\text{H I})$ Modeled (cm^{-2})	$\log(Z_{\text{CGM}})$ [Si/H] (Z_{\odot})
J012528	0.398525	-21.99	285.5 ⁺³⁷ ₋₃₂	12.5 ^{+0.2} _{-0.2}	10.9 ^{+0.2} _{-0.2}	8.69	63.2 ^{+1.7} _{-2.6}	73.4 ^{+4.6} _{-4.7}	163.0	[18.85, 19.00]	18.85 ^{+0.04} _{-0.01}	-1.56 ^{+0.03} _{-0.03}
J035128	0.356992	-20.86	190.9 ⁺⁴⁸ ₋₂₆	12.0 ^{+0.3} _{-0.2}	10.4 ^{+0.3} _{-0.2}	8.63	28.5 ^{+19.8} _{-12.5}	4.9 ^{+33.0} _{-40.2}	72.3	16.86 ± 0.03	16.86 ^{+0.03} _{-0.03}	-0.38 ^{+0.04} _{-0.04}
J040748	0.495164	-19.73	124.4 ⁺⁵² ₋₁₈	11.4 ^{+0.5} _{-0.2}	9.7 ^{+0.5} _{-0.2}	8.46	67.2 ^{+7.6} _{-7.5}	21.0 ^{+5.3} _{-3.7}	107.6	14.34 ± 0.56	14.35 ^{+0.35} _{-0.35}	-1.10 ^{+0.49} _{-0.55}
J045608	0.277938	-19.12	122.0 ⁺⁵⁷ ₋₁₈	11.4 ^{+0.5} _{-0.2}	9.8 ^{+0.5} _{-0.2}	8.14	71.2 ^{+2.6} _{-2.6}	78.4 ^{+2.1} _{-2.1}	50.7	[15.06, 19.00]	15.71 ^{+1.55} _{-0.73}	< -1.40
J045608	0.381511	-20.87	192.3 ⁺⁴⁸ ₋₂₆	12.0 ^{+0.3} _{-0.2}	10.3 ^{+0.3} _{-0.2}	8.67	57.1 ^{+19.9} _{-2.4}	63.8 ^{+4.3} _{-2.7}	103.4	15.10 ± 0.39	15.13 ^{+0.38} _{-0.35}	-0.06 ^{+0.03} _{-0.01}
J045608	0.48382	-21.91	241.8 ⁺³⁸ ₋₂₇	12.3 ^{+0.2} _{-0.2}	10.6 ^{+0.2} _{-0.2}	8.67	42.1 ^{+3.1} _{-3.1}	85.2 ^{+3.7} _{-3.7}	108.0	[16.53, 19.00]	17.65 ^{+0.18} _{-0.17}	-1.32 ^{+0.15} _{-0.15}
J085334	0.163403	-20.56	167.6 ⁺⁴⁸ ₋₂₄	11.9 ^{+0.3} _{-0.2}	10.3 ^{+0.3} _{-0.2}	8.86	70.1 ^{+1.4} _{-0.8}	56.0 ^{+0.8} _{-0.8}	26.2	19.93 ± 0.01	19.93 ^{+0.01} _{-0.01}	-1.70 ^{+0.06} _{-0.05}
J091440	0.244312	-20.55	170.7 ⁺⁴⁹ ₋₂₄	11.9 ^{+0.3} _{-0.2}	10.3 ^{+0.3} _{-0.2}	8.52	39.0 ^{+0.4} _{-0.2}	18.2 ^{+1.1} _{-1.0}	105.9	15.55 ± 0.03	15.55 ^{+0.04} _{-0.03}	-0.78 ^{+0.09} _{-0.10}
J094331	0.2284 ^b	-21.34	216.5 ⁺⁴² ₋₂₇	12.2 ^{+0.2} _{-0.2}	10.6 ^{+0.2} _{-0.2}	8.94 ^c	52.3 ^{+0.3} _{-0.3}	30.4 ^{+0.3} _{-0.4}	123.3	16.03 ± 0.67	16.04 ^{+0.66} _{-0.48}	-1.33 ^{+0.66} _{-0.71}
J094331	0.353052	-19.88	146.8 ⁺⁵⁴ ₋₂₂	11.7 ^{+0.4} _{-0.2}	10.0 ^{+0.4} _{-0.2}	8.53	44.4 ^{+1.1} _{-1.2}	8.2 ^{+3.0} _{-5.0}	96.5	16.46 ± 0.03	16.38 ^{+0.11} _{-0.01}	< -1.69
J095000	0.211866	-21.73	246.9 ⁺³⁶ ₋₂₉	12.4 ^{+0.2} _{-0.2}	10.8 ^{+0.2} _{-0.2}	8.19	47.7 ^{+0.1} _{-0.1}	16.6 ^{+0.1} _{-0.1}	93.6	[16.28, 19.00]	19.00 ^{+0.01} _{-0.09}	-1.48 ^{+0.04} _{-0.02}
J100902	0.227855	-20.19	154.5 ⁺⁵¹ ₋₂₃	11.8 ^{+0.4} _{-0.2}	10.1 ^{+0.4} _{-0.2}	8.52	66.3 ^{+0.6} _{-0.9}	89.6 ^{+1.3} _{-1.3}	64.0	[17.51, 19.00]	18.26 ^{+0.10} _{-0.13}	-2.00 ^{+0.07} _{-0.04}
J113327	0.154599	-19.84	138.8 ⁺⁵² ₋₂₁	11.6 ^{+0.4} _{-0.2}	10.0 ^{+0.4} _{-0.2}	8.19	23.5 ^{+0.4} _{-0.2}	56.1 ^{+1.7} _{-1.3}	55.6	[15.82, 17.00]	16.11 ^{+0.42} _{-0.29}	< -1.98
J113910	0.204194	-19.99	146.1 ⁺⁵² ₋₂₂	11.7 ^{+0.4} _{-0.2}	10.1 ^{+0.4} _{-0.2}	8.67	81.6 ^{+0.4} _{-0.5}	5.8 ^{+0.4} _{-0.5}	93.2	[16.04, 17.00]	16.04 ^{+0.04} _{-0.01}	-0.35 ^{+0.03} _{-0.07}
J113910	0.219724	-17.67	88.7 ⁺⁵² ₋₁₄	11.0 ^{+0.6} _{-0.2}	9.4 ^{+0.6} _{-0.2}	8.37	85.0 ^{+5.0} _{-8.5}	44.9 ^{+8.9} _{-8.1}	122.0	14.20 ± 0.07	14.30 ^{+0.01} _{-0.28}	< 0.63
J113910	0.319255	-20.48	170.4 ⁺⁵¹ ₋₂₉	11.9 ^{+0.3} _{-0.2}	10.2 ^{+0.3} _{-0.2}	8.61	83.4 ^{+1.4} _{-1.1}	39.1 ^{+1.9} _{-1.7}	73.3	16.19 ± 0.03	16.19 ^{+0.03} _{-0.03}	-2.59 ^{+0.58} _{-0.04}
J123304	0.318757	-20.62	176.6 ⁺⁵⁰ ₋₂₅	11.9 ^{+0.3} _{-0.2}	10.3 ^{+0.3} _{-0.2}	8.57	38.7 ^{+1.6} _{-1.8}	17.0 ^{+2.2} _{-2.3}	88.9	15.72 ± 0.02	15.72 ^{+0.02} _{-0.02}	-1.14 ^{+0.13} _{-0.09}
J124154	0.205267	-19.83	140.2 ⁺⁵² ₋₂₁	11.6 ^{+0.4} _{-0.2}	10.0 ^{+0.4} _{-0.2}	8.64	56.4 ^{+0.3} _{-0.5}	77.6 ^{+0.3} _{-0.4}	21.1	[16.63, 19.00]	17.43 ^{+0.02} _{-0.03}	-0.32 ^{+0.05} _{-0.03}
J124154	0.217905	-19.77	138.7 ⁺⁵² ₋₂₁	11.6 ^{+0.4} _{-0.2}	10.0 ^{+0.4} _{-0.2}	8.62	17.4 ^{+1.4} _{-1.6}	63.0 ^{+1.8} _{-2.1}	94.6	15.59 ± 0.12	15.72 ^{+0.09} _{-0.11}	-0.57 ^{+0.16} _{-0.09}
J132222	0.214431	-21.18	204.8 ⁺⁴⁴ ₋₂₆	12.1 ^{+0.3} _{-0.2}	10.5 ^{+0.3} _{-0.2}	8.80	57.9 ^{+0.1} _{-0.2}	13.9 ^{+0.2} _{-0.2}	38.6	[16.97, 19.00]	19.00 ^{+0.01} _{-0.12}	-1.90 ^{+0.04} _{-0.03}
J134251	0.0708 ^b	-18.89	109.1 ⁺⁴⁶ ₋₁₆	11.4 ^{+0.5} _{-0.2}	9.8 ^{+0.5} _{-0.2}	8.86 ^c	57.7 ^{+0.3} _{-0.3}	13.9 ^{+0.2} _{-0.2}	39.4	14.61 ± 0.47	15.33 ^{+0.26} _{-0.69}	-0.02 ^{+0.57} _{-0.33}
J134251	0.227042	-21.77	251.8 ⁺³⁶ ₋₂₉	12.4 ^{+0.2} _{-0.2}	10.8 ^{+0.2} _{-0.2}	8.72	10.1 ^{+0.6} _{-1.0}	13.2 ^{+0.5} _{-0.4}	35.3	18.83 ± 0.05	18.88 ^{+0.06} _{-0.04}	-0.36 ^{+0.04} _{-0.05}
J155504	0.189201	-21.03	193.7 ⁺⁴⁵ ₋₂₅	12.1 ^{+0.3} _{-0.2}	10.5 ^{+0.3} _{-0.2}	8.67	51.8 ^{+0.7} _{-0.7}	47.0 ^{+0.3} _{-0.8}	33.4	[16.37, 19.00]	18.04 ^{+0.01} _{-0.90}	-1.43 ^{+0.71} _{-0.04}
J213135	0.430200	-21.47	199.8 ⁺⁴² ₋₂₅	12.0 ^{+0.3} _{-0.2}	10.4 ^{+0.3} _{-0.2}	8.65	48.3 ^{+3.5} _{-3.7}	14.9 ^{+6.0} _{-4.9}	48.4	19.88 ± 0.10	19.78 ^{+0.01} _{-0.01}	-1.96 ^{+0.03} _{-0.03}
J225357	0.352787	-20.67	180.3 ⁺⁵⁰ ₋₂₅	11.9 ^{+0.3} _{-0.2}	10.3 ^{+0.3} _{-0.2}	8.58	36.7 ^{+6.9} _{-4.6}	88.7 ^{+4.6} _{-4.8}	203.2	14.53 ± 0.05	14.56 ^{+0.02} _{-0.19}	< -0.22

^a The full quasar name along with the quasar and galaxy RA and DEC can be found in [Pointon et al. \(2019a\)](#).

^b Keck ESI galaxy redshifts and metallicities derived from this work and from [Kacprzak et al. \(2018\)](#); [Pointon et al. \(2019a\)](#); [Kacprzak et al. \(2010\)](#).

^c Galaxy redshifts and metallicities obtained from [Werk et al. \(2012\)](#).

([Gonzaga et al. 2012](#)) and cosmic rays were removed during the multidrizzle process when enough frames were available, otherwise L.A.Cosmic was used ([van Dokkum 2001](#)). WFPC2 data were previously reduced using the WFPC2 Associations Science Products Pipeline (WASPP) (see [Kacprzak et al. 2011b](#)). Galaxy morphological parameters were modeled with a two-component disk+bulge model using GIM2D ([Simard et al. 2002](#)), where the disk component has an exponential profile while the bulge has a Sérsic profile with $0.2 \leq n \leq 4.0$. We apply the standard convention of an azimuthal angle $\Phi = 0^\circ$ defined to be along the galaxy projected major axis and $\Phi = 90^\circ$ defined to be along the galaxy projected minor axis.

Galaxy photometry was adopted from [Kacprzak et al. \(2015a\)](#), who used the Source Extractor software (SExtractor; [Bertin & Arnouts 1996](#)) with a detection criterion of 1.5σ above background. The m_{HST} magnitudes in each filter are quoted in the AB system and are listed in Table 1. We adopt calculated halo masses and virial radii from [Ng et al. \(2019\)](#), who applied halo abundance matching methods in the Bolshoi N-body cosmological simulation ([Klypin et al. 2011](#)) see [Churchill et al. \(2013a,b\)](#) for further details. We then calculate stellar masses using abundance matching models from [Moster et al. \(2010\)](#) as described by [Stewart \(2011\)](#).

2.3. Galaxy Spectroscopy

Galaxy spectra were obtained using the Keck Echelle Spectrograph and Imager, ESI, ([Sheinis et al. 2002](#)). Details of the

ESI/Keck observations are presented in [Kacprzak et al. \(2018\)](#) and [Pointon et al. \(2019a\)](#). We binned the CCD by two in the spatial directions resulting in pixel scales of $0.27 - 0.34''$ over the echelle orders of interest. Also, we binned the CCD by two in the spectral direction resulting in a resolution of $22 \text{ km s}^{-1} \text{ pixel}^{-1}$ (FWHM $\sim 90 \text{ km/s}$) for a $1''$ slit. ESI has a wavelength coverage of $4000 - 10,000 \text{ \AA}$, which allows for the detection of multiple emission lines such as [O II] doublet, H β , [O III] doublet, H α , and [N II] doublet.

All ESI data were reduced using IRAF. Galaxy spectra are both vacuum and heliocentric velocity corrected to provide a direct comparison with the quasar spectra. The derived wavelength solution was verified against a catalog of known sky-lines which resulted in a RMS difference of $\sim 0.03 \text{ \AA}$ ($\sim 2 \text{ km s}^{-1}$). The Gaussian fitting software (FITTER: see [Churchill et al. 2000a](#)) was used to simultaneously fit to H α and [N II] emission lines to determine their total flux. The line centers and velocity widths were tied together for the two lines. We compute a gas-phase oxygen abundance for each galaxy using the N2 relation of [Pettini & Pagel \(2004\)](#), where $12 + \log(\text{O}/\text{H}) = 8.90 + 0.57 \times \text{N2}$ ($\text{N2} \equiv \log(\text{N II}/\text{H}\alpha)$). Galaxy ISM metallicities are shown in Table 1.

3. RESULTS

In this section we explore the metallicities of both the galaxy ISM and of the CGM to determine if there is a relationship between distant CGM gas and its host galaxies.

In Figure 1, we present galaxy ISM metallicities as deter-

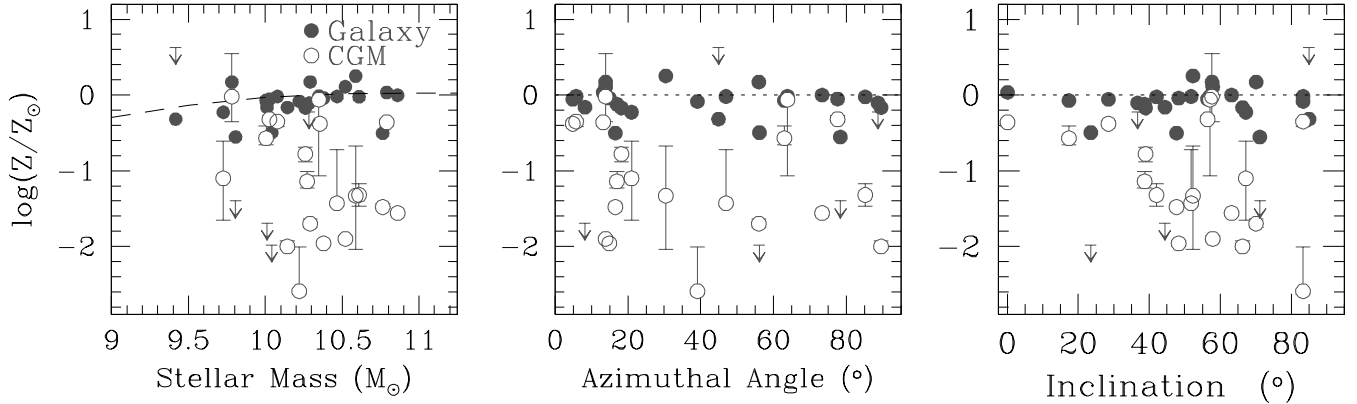


FIG. 1.— (Left) The stellar mass and ISM metallicity relation normalized to the solar oxygen abundance of 8.69 (Asplund et al. 2009). The dashed line is the expected stellar mass-metallicity relation at the mean redshift of our sample $z = 0.28$ (see text for details). The CGM metallicity [Si/H] is also shown as a function of stellar mass, which exhibits large scatter relative to the ISM metallicities at fixed stellar mass. (Middle) ISM and CGM metallicities as a function of azimuthal angle and (Right) inclination angle. As expected the ISM metallicities are flat as a function of azimuthal and inclination angle while the CGM metallicity exhibits large ~ 2 dex of scatter.

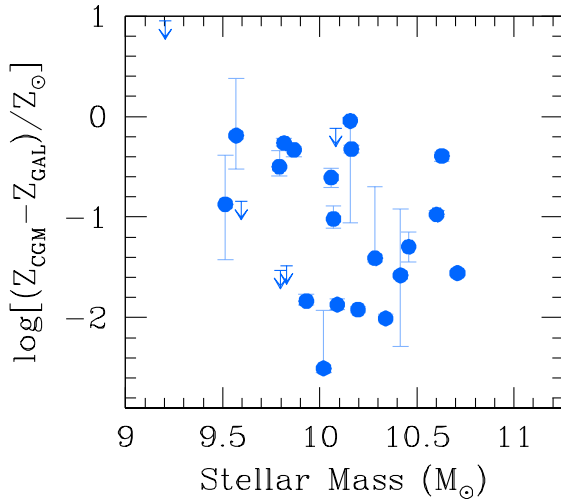


FIG. 2.— The difference between the CGM and galaxy ISM metallicities as a function of host galaxy stellar mass. All but one system has CGM metallicity higher than the galaxy metallicity. The 21 CGM metallicity measurements exhibit a mean offset from the galaxy metallicity by $\log(dZ) = -1.17 \pm 0.11$ where the error is quoted as the standard error in the mean. The scatter in this difference can be expressed by the standard deviation of $1\sigma = 0.72$. This metallicity difference is independent of stellar mass over the small range examined here.

mined from the $H\alpha$ and NII line ratios normalized to oxygen solar abundance of 8.69 (Asplund et al. 2009). Here $\log(Z)$ is defined for galaxies as the ratio of the mass of oxygen in the gas-phase and the hydrogen gas mass. Our sample of galaxies have a stellar mass range from $9.4 \leq \log(M_*/M_\odot) \leq 10.9$ with roughly 0.5 dex error on the stellar mass. The dashed line shows the galaxy mass-metallicity relation obtained from the formalism of Zahid et al. (2014) evaluated at our mean galaxy redshift of $z = 0.28$ and then normalized to the solar oxygen abundance. We also normalize the Zahid et al. (2014) relation to the $N2$ Pettini & Pagel (2004) calibration used to calculate our galaxy ISM metallicities following the methods of Kewley & Ellison (2008)⁷.

⁷ Note Zahid et al. (2014) used the Kobulnicky & Kewley (2004) calibra-

We find that our galaxy ISM metallicities agree with the expectations and follow the general trend of increasing metallicity with increasing mass having a 1σ scatter of 0.19 dex about the relation. This scatter could be further reduced if the mass-metallicity relation was computed for the full range of galaxy redshifts observed here, however this is beyond the scope of this paper and not necessary for our analysis.

While the galaxy metallicities exhibit a tight relation with stellar mass (0.19 dex scatter), the metallicity of the CGM shows no dependence with stellar mass and exhibits a scatter that ranges over 2 dex. This clearly shows that the CGM is more complex and the metallicity is likely driven by a range of processes compared to that of the ISM. In all cases, except for a poorly constrained limit, the CGM metallicity is always lower than the galaxy ISM metallicity. Figure 2 shows the difference between the CGM and galaxy ISM metallicities as a function of host galaxy stellar mass. Using a survival analysis with all of the data we find that the CGM metallicity is offset from the galaxy metallicity by $\log(dZ) = -1.17 \pm 0.11$ where $\log(dZ)$ is quoted as the mean offset from the galaxy metallicity while the error is quoted as the standard error in the mean. The scatter in this difference can be expressed by the standard deviation of $1\sigma = 0.72$. This metallicity difference is independent of stellar mass over the small range examined here. The relative CGM and ISM metallicities for the stellar mass range of $9.7 \leq M_* < 10.3$ and $10.3 \leq M_* \leq 10.8$ exhibit metallicity differences of -1.27 ± 0.14 (1σ scatter of 0.91) and -1.09 ± 0.17 (1σ scatter of 0.67), respectively, with values quoted as the mean difference while the error is quoted as the standard error in the mean. We have also applied generalized Kendall and Spearman rank correlation tests, which accounts for measured limits in the sample (Feigelson & Nelson 1985), between the stellar mass and $\log(dZ)$. We no strong supporting evidence for trends between stellar mass and $\log(dZ)$ (2.1σ – Kendall, 2.3σ – Spearman).

Given that our sample is low redshift ($\langle z \rangle = 0.28$), where one could expect metal-poor accretion to be minimal and metals within the CGM could be well mixed or metal enriched from Gyrs of ongoing outflows, there is still a significant metallicity difference between the host galaxy and the CGM. Further-

tion and the difference between these calibration methods can lead to offset of ~ 0.3 dex in metallicity.

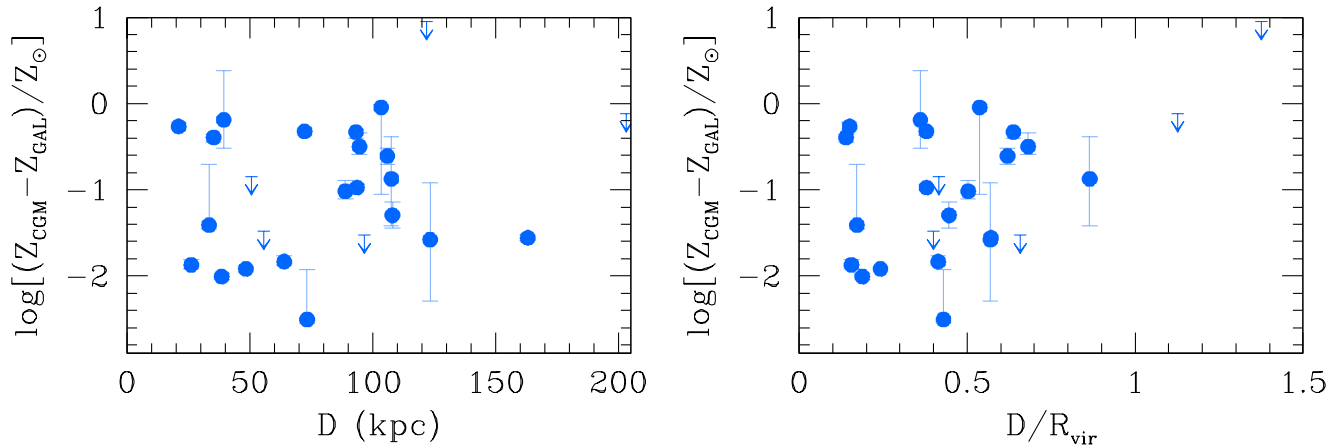


FIG. 3.— The difference between the CGM and galaxy ISM metallicities shown as function of impact parameter (left) and as a function of the fraction of the virial radius (right). All of the CGM measurements reside within 200 kpc and most within $1 R_{vir}$ of their host galaxies. Arrows represent limits on the CGM metallicities. Note the large scatter at all distances away from the galaxy with no obvious metallicity gradient.

more, this difference is independent of stellar mass.

The middle and right panels of Figure 1 show both the galaxy and CGM metallicities as a function of the azimuthal and inclination angles, respectively. As expected, the galaxy ISM metallicity is independent of the galaxy orientation with respect to the quasar sight-line as well as the galaxy’s inclination angle. The CGM however exhibits large scatter as a function of azimuthal angle and inclination angle as previously shown by Pointon et al. (2019a) using a larger sample of 47 galaxy-absorber pairs. Pointon et al. (2019a) explored how the CGM metallicity behaves relative to the galaxy inclination and azimuthal angles and found no apparent trend, which conflicts with a scenario of planer accretion and bi-polar outflows (e.g., Nelson et al. 2019). However, the Pointon et al. study did not address how the relative galaxy-CGM metallicity behaves as a function of orientation or impact parameter.

It is unclear how we expect the CGM metallicity to behave as a function of impact parameter. Simulations predict coplaner accretion with bi-conical outflows (e.g., Nelson et al. 2019) and negative radial metallicity gradients for both outflow and accretion models (e.g., van de Voort & Schaye 2011). Furthermore, simulations of extended disk ISM metallicities show that galaxies have negative metallicity gradients extending out to 10–20 kpc (e.g., Kobayashi & Nakasato 2011; Pilkington et al. 2012), while observations show either flat or negative gradients with significant scatter in their slopes (e.g., Wuyts et al. 2016; Sánchez-Menguiano et al. 2018).

In the left panel of Figure 3, we present the difference in metallicity between the CGM and galaxy as a function of impact parameter. All of our absorption systems are within 200 kpc of the host galaxy. We find no apparent metallicity gradient ($0.78\sigma - \text{Kendall}$, $0.92\sigma - \text{Spearman}$) with a larger scatter of low and high metallicity systems at all distances away from the galaxy. It is interesting to note that the two lowest metallicity systems reside within 75 kpc (or within $0.5R_{vir}$) of the host galaxy, which is counter-intuitive since one might expect these more unpolluted systems to reside further away from their host galaxies (unless metal-poor accretion is really reaching low impact parameters without mixing).

It is more meaningful to show the difference in ISM/CGM metallicities as a function of the the fraction of the virial radius given that these galaxies cover a range of halo masses. In

the right panel of Figure 3 shows the difference between CGM and ISM metallicities as a function of the fraction of the virial radius. Almost all of our absorption systems, except for two limits, reside within $1 R_{vir}$ of their host galaxies. Again, we find no strong trend between metallicity and the fraction of the virial radius ($1.63\sigma - \text{Kendall}$, $1.51\sigma - \text{Spearman}$). While the most metal poor absorbers reside near to the galaxy, there is significant scatter at all radii. The scatter seen here could be a result of gas being enriched from outflows, while metal-poor gas could come from accreting gas. All of these might be expected to have an orientation dependence.

In the left panel of Figure 4 we present the difference between the CGM and galaxy ISM metallicities as a function of azimuthal angle. In a simple CGM scenario, one may expect that metal-poor gas relative to the galaxy should accrete along the major axis of the galaxy disk, which should populate the lower left corner of the plot. On the other hand, metal-enriched outflows relative to the host galaxy should occur along the galaxy minor axis, which should populate the upper right corner of the plot. However, it is clear from the figure that there is a large range in $\log(dZ)$ from 0 to -2 at all azimuthal angles. We find that the mean metallicity difference between the CGM and host galaxy for both along the major and minor axes, bifurcated at 45 degrees, are -1.13 ± 0.18 (1σ scatter of 0.76) and -1.23 ± 0.11 (1σ scatter of 0.65), respectively.

It does seem clear that there is no significant relative metallicity dependence as a function of azimuthal angle. This is consistent with the results of Pointon et al. (2019a) who showed that the CGM metallicity alone does not have a metallicity dependence. When taking into account the host galaxy metallicity, this does not unveil a new result. This is consistent with the first suggestive results of Péroux et al. (2016) using 9 galaxy absorber pairs. Given that there exists a large scatter in CGM metallicities, while ISM metallicities show very little scatter, then it is not surprising no additional relationships are discovered here. It is also interesting to note that the most metal enriched systems are along the major axis of the galaxy and not the minor axis, where outflows are expected to dominate. So it is unclear what is the source of these high metallicity systems and/or if they are part of a very extended HI disk. It is plausible that recycled metal-enriched

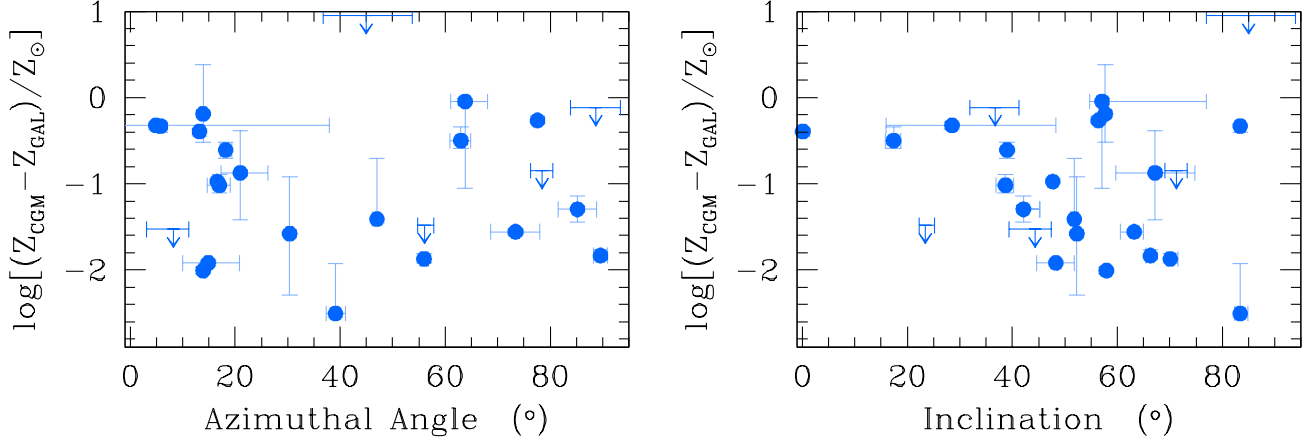


FIG. 4.— The difference between the CGM and galaxy ISM metallicities as a function of azimuthal angle (left) and galaxy inclination (right). In a simple CGM model, we would expect low metallicity gas to accrete along the major axis (bottom left corner of the plot) while higher metallicity gas outflows along the minor axis (upper right corner of the plot). When taking the galaxy metallicity into account, we do not find a correlation with azimuthal angle as expected from the simple model. There exists a range of metallicities at all azimuthal angles. (Right) As a galaxy becomes more edge-on, it is expected that outflows and accretion signatures would be more apparent than for near face-on galaxies. We do find that highly inclined galaxies have a range of metallicities that could arise from outflow and/or accretion signatures.

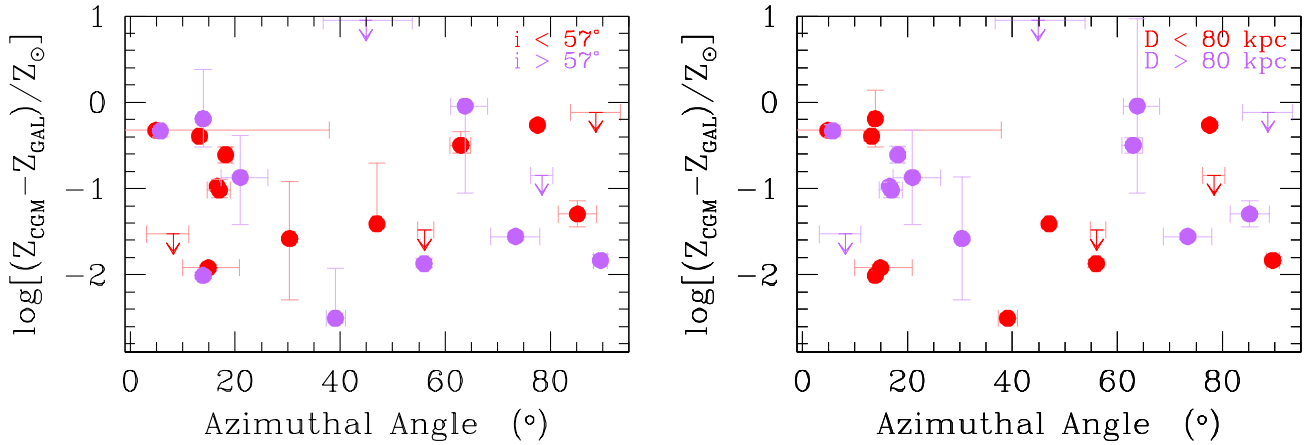


FIG. 5.— Same as left panel of Figure 4 except now the data are color-coded as a function of high and low inclination angles (left) and high and low impact parameters (right). Note that regardless of low or high inclination, or low and high impact parameter, there is no correlation with the relative ISM-CGM metallicity and azimuthal angle.

gas could fall back towards the galaxy and reaccrete along the major axis, which could explain the large scatter seen at low azimuthal angles. However, it is puzzling that there exists absorption systems that have much lower metallicities than their host galaxies along the minor axis.

The right hand panel of Figure 4 shows the relative metallicity as a function of galaxy inclination. We do not have many near face-on galaxies in our sample, so we are unable to comment on the distribution of metallicities here. However, in a simple inflow/outflow scenario, one would assume that these gas flows may be more distinguishable for edge-on galaxies. At intermediate to highly inclined galaxies, we find significant scatter ranging from $0 \lesssim \log(dZ) \lesssim -2$. This further indicates that there is likely no metallicity dependence on galaxy inclination.

It could be possible that combination of inclination angles and/or impact parameters could dilute any correlation between the relative galaxy ISM and CGM metallicities as a

function of azimuthal angle. In Figure 5 we explore the azimuthal dependence of the relative metallicity bifurcated by high and low galaxy inclination angles at 57 degrees, which splits the sample roughly equally into two subsets. For highly inclined galaxies, we would expect to see the strongest relation between relative metallicity and azimuthal angle since the quasar sight-line should only pass through individual outflow and accretion structures and not a blend of the two in projection. We find a similar scatter in metallicity for both low and high inclination galaxies. Interestingly, we find the lowest metallicities relative to their host galaxies tend to be highly inclined and exist over the full range of azimuthal angles. Low inclination galaxies have fewer very metal-poor CGM systems which could be due to an averaging of structures and gas metallicities along the quasar sight-line (i.e., passing through both outflows and accreting gas).

The right panel of Figure 5 also shows the azimuthal metallicity dependence as a function of low ($D < 80$ kpc) and high

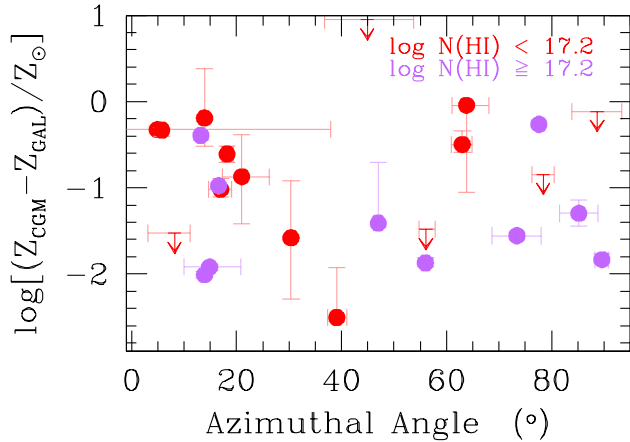


FIG. 6.— Same as Figure 5 except now the data are color-coded as a function of low ($\log N(\text{H I}) < 17.2$) and high ($\log N(\text{H I}) \geq 17.2$) modeled H I column densities.

($D > 80$ kpc) impact parameters. Since it has been shown that outflows may only extend out to 50–100 kpc (e.g., [Bordoloi et al. 2011](#); [Lan & Mo 2018](#)), one could expect the highest metallicity systems, or at least metal-enriched systems (at or above the galaxy ISM metallicity), to exist at low impact parameters and possibly along the galaxy minor axis. We find that along the minor axis, both low and high impact parameter systems have a range of metallicities. In fact, the three low metallicity systems at low impact parameters, which is unexpected. Again, along the major axis, both low and high impact parameter systems have a range of relative CGM to galaxy metallicity. Therefore impact parameter doesn’t seem to play a critical role in the azimuthal dependence for the metallicity difference between the CGM and the host galaxies. We do find that intermediate azimuthal angles are dominated by $D < 80$ kpc systems, where possibly extended disk or interactions may also contribute to the absorption detected here.

It is further possible that any azimuthal dependence could be driven by the hydrogen column density since the CGM metallicity bi-modality is only shown for pLLSs and LLSs ([Wotta et al. 2016, 2019](#)). In Figure 6 we show the ISM-CGM metallicity difference versus azimuthal angle separated into high $N(\text{H I})$ ($\log N(\text{H I}) \geq 17.2$ – purple) and low $N(\text{H I})$ ($\log N(\text{H I}) < 17.2$ – red). In this figure high column density systems tend to have lower metallicities, which is consistent with previous work (see [Pointon et al. 2019a](#)). The vast majority of low column density systems (10/15 – red points in Figure 6) reside along the galaxy major axis and only four low column density systems with metal-line measurements are found at greater than ~ 60 degrees. This could be suggestive that low $N(\text{H I})$ systems are better tracers of accretion if the accreting gas has a range of metallicities, however more data is required. It is also possible that low $N(\text{H I})$ gas along the major axis of galaxies occurs as both metal-poor gas accretion and metal-enriched recycling.

We also find that 6/10 high column density systems (purple points in Figure 6) reside above an azimuthal angle of 40 degrees, suggesting that high column density systems could better trace outflows. However, the metallicities along the major and minor axes are consistent with each other.

4. DISCUSSION

Simulations clearly show that the CGM is complex, yet observations have shown that the spatial distribution of high and low ions are azimuthally dependent ([Bouché et al. 2012](#); [Kacprzak et al. 2012a](#); [Lan et al. 2014](#); [Kacprzak et al. 2015a](#); [Lan & Mo 2018](#)). Even the internal dispersion of the CGM absorption for low ions points to accretion and outflow scenarios ([Nielsen et al. 2015](#)). Furthermore, relative gas and galaxy kinematics show that low ions are kinematically connected to their host galaxy by aligning with their rotation curves and being modelled well by accreting+corotating gas ([Steidel et al. 2002](#); [Kacprzak et al. 2010, 2011a](#); [Ho et al. 2017](#); [Martin et al. 2019](#); [Zabl et al. 2019](#)). On the other hand, minor axis gas also seems to be well modelled by outflowing gas ([Bouché et al. 2012](#); [Gauthier & Chen 2012](#); [Schroetter et al. 2016](#)). Finally, the metallicity distribution of LLS and pLLS appears bimodal, which also suggests that outflows and accretion are dominant phenomena within the CGM ([Wotta et al. 2016, 2019](#)). Thus the spatial distribution of metallicity around galaxies seemed to be key to understanding the origins of the CGM.

However, as [Pointon et al. \(2019a\)](#) has shown, CGM metallicity alone has no correlation with azimuthal angle or inclination regardless of impact parameter, $N(\text{H I})$, etc. This is quite disappointing given the simple picture presented by observations. However, we do not know how the relative galaxy-ISM and CGM metallicities affect these results given the well-known galaxy stellar mass and ISM metallicity relation found at all redshifts (e.g. [Tremonti et al. 2004](#); [Sanders et al. 2014](#); [Steidel et al. 2014](#); [Zahid et al. 2014](#); [Kacprzak et al. 2015b](#)). Thus accounting for the galaxy metallicity could enhance any possible relationship with metallicity and galaxy orientation. Here we examine these relationships using 25 systems with both galaxy ISM and CGM metallicities.

We find that although host galaxies follow a stellar mass metallicity relation (0.19 dex scatter over the mass range $9.4 \leq \log(M_*/M_\odot) \leq 10.9$), the CGM is quite scattered as a function of stellar mass spanning 2 dex in metallicity. This is expected as galaxy ISM metallicities are driven by stellar evolution and gas accretion and are averaged over entire galaxy disks while the CGM detected along point-like quasar sightlines may originate from IGM gas accretion, from nearby galaxies/satellites, or from recycled and outflowing gas generated from within the galaxy. We find that the mean of the CGM metallicities are lower than the mean galaxy metallicities by -1.17 ± 0.11 . This offset is independent of stellar mass over the small range examined here. The mean CGM metallicities for stellar mass ranges of $9.7 \leq \log(M_*/M_\odot)_* < 10.3$ and $10.3 \leq \log(M_*/M_\odot)_* \leq 10.8$ are lower than the galaxy metallicity by -1.27 ± 0.14 (1σ scatter of 0.91) and -1.09 ± 0.17 (1σ scatter of 0.67), respectively. Thus there is a significant difference between the host galaxy and the CGM metallicities, which are stellar mass independent. There may be a small hint of a correlation with stellar mass and $\log(dZ)$ but it is not highly significant (2.1σ – Kendall, 2.3σ – Spearman).

These results are consistent with the findings of [Prochaska et al. \(2017\)](#) who has shown that the CGM metallicity does not correlate with the ISM metallicity of host galaxies nor does the CGM metallicity correlate with stellar mass. However, it is difficult to compare our works directly since they use the [Haardt & Madau \(2012\)](#) (HM12) ionizing background. Previous works have shown that harder spectrum of ionizing photons from the HM12 background is due to a lower escape frac-

tion of radiation from galaxies compared to the HM05 background, which leads to higher metallicity estimates and an anti-correlation between N(HI) and metallicity (Howk et al. 2009; Werk et al. 2014; Wotta et al. 2016, 2019; Chen et al. 2017; Zahedy et al. 2019; Pointon et al. 2019a).

All of our CGM metallicities are lower than the galaxy ISM metallicities. This could imply that CGM may originate from a nearby satellite galaxy or its outflow or tidal debris. However, the halo gas cross-section of satellite galaxies are predicted to be extremely small (Gauthier et al. 2010; Martin et al. 2012; Tumlinson et al. 2013) and thus, an unlikely contributor to the bulk of the detected absorption.

The lower CGM metallicities could imply that gas ejected from galaxies is diluted with metal poor gas within the CGM or metals ejected from host galaxies have taken a long time to travel out into the CGM. If the gas does take a long time to travel out into the CGM, an interesting experiment is to then see at what age of the Universe did a $z = 0.28$ $M_* \sim 10^{10.5} M_\odot$ galaxy have a ISM metallicity that was -1.2 dex lower than its current value. We estimate this gas must have been ejected prior to $z = 3$ given the limits of the stellar mass evolution of $\sim 10^{10.5} M_\odot$ galaxy (Papovich et al. 2015) and combined with the evolution of the mass-metallicity relation (Mannucci et al. 2009; Zahid et al. 2014). Thus, the gas would have to be ejected roughly at >8 Gyr prior to $z = 0.28$ in order to have a galaxy such a low metallicity. This large time-scale provides ample time for ejected gas to travel out into the CGM and also recycle back to the disk since this is estimated to take at least 1 Gyr (e.g., Oppenheimer & Davé 2009; Oppenheimer et al. 2010). However, this also assumes no gas mixing, which would likely further change the metallicity of the ejected material. So it seems possible that any metal poor gas that was ejected at early times should have been enriched several times over a >8 Gyr time-frame. Thus, in order to find low metallicity systems along the minor axis of galaxies, outflowing gas would have to be well-mixed with its metal-poor surroundings within the CGM or maybe the cool CGM is not a good tracer of galactic outflows.

Péroux et al. (2016) first looked into the difference between the galaxy ISM and CGM metallicities as a function of azimuthal angle with nine galaxies and suggested that there seems to be a large scatter along the major axis while they only had two lower relative metallicity systems along the minor axis. We further find that the mean metallicity differences along the major and minor axes, bifurcated at 45 degrees, are -1.13 ± 0.18 (1σ scatter of 0.76) and -1.23 ± 0.11 (1σ scatter of 0.65), respectively. Regardless of whether we examine our sample by low/high inclination or low/high impact parameter, or low/high column density (or any combination of these), we do not find any significant relationship with relative metallicity and azimuthal angle.

So what is going on here and should we be focusing on metallicity when examining modes of accretion and outflows? Outflows do occur and there is plenty of evidence that they likely occur along the minor axis and this gas has to be metal-enriched. Also, some form of accretion must happen given all the kinematic evidence found for CGM-galaxy pairs and that fact that galaxies continue to form stars. Yet it is unclear what the metallicity of that accreting gas could be. Cosmological simulations predict that gas accretion metallicities range between $10^{-3} - 10^{-0.5} Z_\odot$, which is dependent on redshift and halo mass (Kereš et al. 2005; Fumagalli et al. 2011a; Oppenheimer et al. 2012; van de Voort & Schaye 2011; Shen

et al. 2013; Kacprzak et al. 2016), however this range does overlap with the expected metallicities of recycled/outflowing gas. Also, the complexity of outflowing gas makes things worse given there is typically hot outflowing material containing cool entrained clouds. Thus maybe metallicity alone is a poor indicator of the origins of the CGM gas or the metallicity of low ions might be a poor indicator of the metallicity of hot outflowing gas.

Analysis of cosmological simulations from Ford et al. (2014) showed that low-ionization metal absorbers tend to arise within inflowing gas, while high-ionization metal absorbers trace ancient outflowing gas deposited in galaxy haloes many Gyr ago. (Muzahid et al. 2015) showed a galaxy having both a metal-poor low ionization component (~ -1.5) and a high ionization metal rich component (> 0.3). They concluded that the low ionization metal-poor phase was consistent with being recycled material in the galaxy halo and that the high-ionization, metal-enriched, low density gas presumably originated from star-formation driven outflows from the host-galaxy. Thus it is possible that different gas phases have different origins and given this example, more work is needed to further model the multi-phase CGM metallicities.

It is still puzzling however that pLLSs and LLSs have bimodal metallicity distribution and this needs to be explored within simulations and determined whether the bimodality is caused by internal CGM properties or due to environmental effects. So far cosmological simulations have been unable to reproduce the CGM metallicity bimodality (Hafen et al. 2017, 2018; Rahmati & Oppenheimer 2018; Lehner et al. 2019). Furthermore environmental effects may not be the likely mechanism producing the bimodality either (Pointon et al. 2019b). It seems that properties such as velocities, column densities and equivalent widths that are straight forward to measure provide the most fruitful evidence for gas flows.

On the other hand, modelling the total metallicity along a given sight-line is not straightforward either and can lead to confusing results. We know that the CGM metallicity must vary along the sight-lines (Churchill et al. 2015; Peebles et al. 2018), however most studies model a global single-phase metallicity since it is difficult in most cases to assign the correct amount of hydrogen to given metal features from different gas phases in a single spectrum. Lehner et al. (2019) has shown for ~ 30 near redshift-separated absorbers (separations of $50-400$ km s^{-1}) have metallicities differences ranging from 0 to 1.7dex. Only a smaller number of absorption-line systems have been modeled as multi-phase and with cloud-to-cloud metallicities (e.g., Prochter et al. 2010; Tripp et al. 2011; Crighon et al. 2013b; Muzahid et al. 2015, 2016; Rosenwasser et al. 2018; Zahedy et al. 2019). Furthermore, it is expected that absorption arising from outflows would have large cloud-to-cloud variations in metallicity and ionization level (e.g., Veilleux et al. 2005; Rosenwasser et al. 2018; Zahedy et al. 2019), which we are averaging over. We are also metal-biased in that detecting some metals at a given velocity does not imply there is no metal poor gas at that same velocity in some other spatial location along the sight-line that is masked by those other metal lines. Maybe the CGM is not well mixed and metallicity is not a great indicator of dynamic processes and we are best to focus our efforts on dynamic/kinematic measurements to study gas flows.

Either way, larger and well targeted samples may provide future insight to the metallicity distribution around galaxies.

5. CONCLUSIONS

We present galaxy ISM and CGM metallicities for 25 absorption systems associated with isolated star-forming galaxies ($0.07 \leq z \leq 0.50$). Galaxy ISM metallicities were measured using H α and [NII] emission lines obtained from Keck/ESI spectra. The CGM metallicities were adopted from Pointon et al. (2019a), which were modeled using an MCMC analysis along with Cloudy. We examine the galaxy mass metallicity relation for our galaxies and their absorption systems. We also explore whether the relative galaxy ISM and CGM metallicity correlates with galaxy orientation with respect to the quasar. Our results are summarized as follows:

1. We find that our galaxy ISM metallicities agree with the expectations of following the general trend of increasing metallicity with increasing stellar mass having a 1σ scatter of 0.19 dex about the relation determined at $\langle z \rangle = 0.28$. This scatter could be further reduced if the mass-metallicity relation was computed for the full range of galaxy redshifts in our sample.
2. CGM metallicity shows no dependence with stellar mass ($< 2.3\sigma$ significance) and exhibits a scatter that ranges over 2 dex. The CGM and galaxy metallicity differences for stellar mass ranges of $9.7 \leq M_* < 10.3$ and $10.3 \leq M_* \leq 10.8$ are -1.27 ± 0.14 (1σ scatter of 0.91) and -1.09 ± 0.17 (1σ scatter of 0.67), respectively. Thus, even at low redshift, where one might expect the global metallicities to be more homogenized, there is still a significant difference between the host galaxy ISM and the CGM metallicities and are stellar mass independent
3. The CGM metallicities are always lower than the galaxy ISM metallicities and are offset by $\log(dZ) = -1.17 \pm 0.11$ where $\log(dZ)$ is quoted as the mean offset from the galaxy metallicity while the error is quoted as the standard error in the mean. The scatter in this offset can be expressed by the standard deviation of $1\sigma = 0.72$.
4. All of our CGM measurements reside within 200 kpc and $1.5 R_{vir}$ of their host galaxies. We find no obvious metallicity gradient as a function of impact parameter or virial radius ($< 1.6\sigma$ significance). This could be diluted with a range of galaxy orientations within that sample. Ideally, this sort of work would best be done for a large sample of edge-on galaxies.
5. There is no relative CGM–galaxy metallicity as a function of azimuthal angle. We find that the mean metallicity differences along the major and minor axes, bifurcated at 45 degrees, are -1.13 ± 0.18 (1σ scatter of 0.76) and -1.23 ± 0.11 (1σ scatter of 0.65), respectively.
6. Regardless of whether we examine our sample by low/high inclination or low/high impact parameter, or low/high H I column density (or any combination of these), we do not find any significant relationship with relative CGM–galaxy metallicity and azimuthal angle.
7. The majority of low column density systems ($10/15 - \log N(\text{H I}) < 17.2$) reside along the galaxy major axis and only two low column density systems with metal-line measurements are found at ~ 60 degrees. We also find that 6/10 high column density systems ($\log N(\text{H I}) \geq$

17.2) reside above an azimuthal angle of 40 degrees, suggesting that high column density systems could better trace outflows. However, the metallicities along the major and minor axes are consistent. This could be suggestive that low N(H I) systems are better tracers of accretion if the accreting gas has a range of metallicities. More data is required to determine whether these trends really do exist.

It is undoubtedly true that the CGM is complex. The community has put forth a large body of work showing evidence for accretion and outflows, however a clear confirmation of cosmological accretion remains elusive. CGM metallicities and metallicity differences between the galaxy-ISM to CGM do not help illuminate our understanding of the CGM, at least with current sample sizes. We further need to address how assuming averaged line of sight metallicities and/or single phase metallicities truly effects our results.

An additional issue is that our point-source quasars probe through individual galaxy halos, which could give rise to large variations in metallicity within the halo and along the sight-line. Hopefully in the future, we will be able to use background galaxies, or gravitational lenses (e.g., Lopez et al. 2018) to obtain a better sampling of the halo metallicities and to be less susceptible to line-of-sight variations. For now, it seems that properties such as velocities, column densities and equivalent widths that are easy to measure provide the most fruitful evidence for gas flows.

We thank Roberto Avila (STScI) for his help and advice with modeling PSFs with ACS and WFC3. GGK and NMN acknowledges the support of the Australian Research Council through a Discovery Project DP170103470. Parts of this research were supported by the Australian Research Council Centre of Excellence for All Sky Astrophysics in 3 Dimensions (ASTRO 3D), through project number CE170100012. CWC and JCC are supported by NASA through grants HST GO-13398 from the Space Telescope Science Institute, which is operated by the Association of Universities for Research in Astronomy, Inc., under NASA contract NAS5-26555. CWC and JCC are further supported by NSF AST-1517816. Most of the data presented here were obtained at the W. M. Keck Observatory, which is operated as a scientific partnership among the California Institute of Technology, the University of California, and the National Aeronautics and Space Administration. The Observatory was made possible by the generous financial support of the W. M. Keck Foundation. Observations were supported by Swinburne Keck programs 2016A_W056E, 2015B_W018E, 2014A_W178E and 2014B_W018E. The authors wish to recognize and acknowledge the very significant cultural role and reverence that the summit of Mauna Kea has always had within the indigenous Hawaiian community. We are most fortunate to have the opportunity to conduct observations from this mountain. Based on observations made with the NASA/ESA Hubble Space Telescope, and obtained from the Hubble Legacy Archive, which is a collaboration between the Space Telescope Science Institute (STScI/NASA), the Space Telescope European Coordinating Facility (ST-ECF/ESA) and the Canadian Astronomy Data Centre (CADNRC/CSA).

Facilities: Keck II (ESI) HST (COS, WFPC2, ACS, WFC3).

REFERENCES

- Asplund, M., Grevesse, N., Sauval, A. J., & Scott, P. 2009, *ARA&A*, 47, 481
- Bertin, E., & Arnouts, S. 1996, *A&AS*, 117, 393
- Bordoloi, R., Lilly, S. J., Knobel, C., et al. 2011, *ApJ*, 743, 10
- Bouché, N., Finley, H., Schroetter, I., et al. 2016, *ApJ*, 820, 121
- Bouché, N., Hohensee, W., Vargas, R., Kacprzak, G. G., et al. 2012, *MNRAS*, 426, 801
- Bouché, N., Murphy, M. T., Kacprzak, G. G., et al. 2013, *Science*, 341, 50
- Bouché, N., Murphy, M. T., Péroux, C., Csabai, I. & Wild, V. 2006 *MNRAS*, 371, 495
- Carswell, R. F., & Webb, J. K. 2014, *Astrophysics Source Code Library*, ascl:1408.015
- Chen, H.-W., Lanzetta, K. M., Webb, J. K., & Barcons, X. 2001, *ApJ*, 559, 654
- Chen, H.-W., Kennicutt, R. C., Jr., & Rauch, M. 2005, *ApJ*, 620, 703
- Chen, H.-W., & Mulchaey, J. S. 2009, *ApJ*, 701, 1219
- Chen, H.-W., Johnson, S. D., Zahedy, F. S., et al. 2017, *ApJ*, 842, L19
- Churchill, C. W., Kacprzak, G. G., Steidel, C. C., et al. 2012, *ApJ*, 760, 68
- Churchill, C. W., Mellon, R. R., Charlton, J. C., Jannuzi, B. T., Kirhakos, S., Steidel, C. C., & Schneider, D. P. 2000a, *ApJS*, 130, 91
- Churchill, C. W., Nielsen, N. M., Kacprzak, G. G., & Trujillo-Gomez, S. 2013, *ApJ*, 763, L42
- Churchill, C. W., Trujillo-Gomez, S., Nielsen, N. M., & Kacprzak, G. G. 2013, *ApJ*, 779, 87
- Churchill, C. W., Vander Vliet, J. R., Trujillo-Gomez, S., Kacprzak, G. G., & Klypin, A. 2015, *ApJ*, 802, 10
- Coil, A. L., Weiner, B. J., Holz, D. E., et al. 2011, *ApJ*, 743, 46
- Cooksey, K. L., Prochaska, J. X., Chen, H.-W., Mulchaey, J. S., & Weiner, B. J. 2008, *ApJ*, 676, 262
- Crighton, N. H. M., Bechtold, J., Carswell, R. F., et al. 2013, *MNRAS*, 433, 178
- Crighton, N. H. M., Hennawi, J. F., Simcoe, R. A., et al. 2015, *MNRAS*, 446, 18
- Crighton, N. H. M., Hennawi, J. F., & Prochaska, J. X. 2013, *ApJ*, 776, L18
- Danforth, C. W., Stocke, J. T., & Shull, J. M. 2010, *ApJ*, 710, 613
- Dekker, H., D'Odorico, S., Kaufer, A., Delabre, B., & Kotzłowski H. 2000, *SPIE*, 4008, 534
- Feigelson, E. D., & Nelson, P. I. 1985, *ApJ*, 293, 192
- Ferland, G. J., Porter, R. L., van Hoof, P. A. M., et al. 2013, *Rev. Mexicana Astron. Astrofis.*, 49, 137
- Ford, A. B., Davé, R., Oppenheimer, B. D., et al. 2014, *MNRAS*, 444, 1260
- Fumagalli, M., Cantalupo, S., Dekel, A., et al. 2016, *MNRAS*, 462, 1978
- Fumagalli, M., O'Meara, J. M., & Prochaska, J. X. 2011, *Science*, 334, 1245
- Gauthier, J.-R., & Chen, H.-W. 2012, *MNRAS*, 424, 1952
- Gauthier, J.-R., Chen, H.-W., & Tinker, J. L. 2010, *ApJ*, 716, 1263
- Gonzaga, S., Hack, W., Fruchter, A., Mack, J., eds. 2012, *The DrizzlePac Handbook*. (Baltimore, STScI)
- Haardt, F., & Madau, P. 2012, *ApJ*, 746, 125
- Hafen, Z., Faucher-Giguere, C.-A., Anglés-Alcázar, D., et al. 2018, arXiv:1811.11753
- Hafen, Z., Faucher-Giguère, C.-A., Anglés-Alcázar, D., et al. 2017, *MNRAS*, 469, 2292
- Ho, S. H., Martin, C. L., Kacprzak, G. G., & Churchill, C. W. 2017, *ApJ*, 835, 267
- Howk, J. C., Ribaldo, J. S., Lehner, N., et al. 2009, *MNRAS*, 396, 1875
- Johnson, S. D., Chen, H.-W., & Mulchaey, J. S. 2013, *MNRAS*, 434, 1765
- Kacprzak, G. G. 2017, *Gas Accretion onto Galaxies*, 430, 145
- Kacprzak, G. G., Churchill, C. W., Barton, E. J., & Cooke, J. 2011a, *ApJ*, 733, 105
- Kacprzak, G. G., Churchill, C. W., Ceverino, D., Steidel, C. C., Klypin, A., & Murphy, M. T. 2010, *ApJ*, 711, 533
- Kacprzak, G. G., Churchill, C. W., Evans, J. L., Murphy, M. T., & Steidel, C. C. 2011b, *MNRAS*, 416, 3118
- Kacprzak, G. G., Murphy, M. T., & Churchill, C. W. 2010b, *MNRAS*, 406, 445
- Kacprzak, G. G., Churchill, C. W., & Nielsen, N. M. 2012, *ApJ*, 760, L7
- Kacprzak, G. G., Martin, C. L., Bouché, N., et al. 2014, *ApJ*, 792, L12
- Kacprzak, G. G., Muzahid, S., Churchill, C. W., Nielsen, N. M., & Charlton, J. C. 2015, *ApJ*, 815, 22
- Kacprzak, G. G., Yuan, T., Nanayakkara, T., et al. 2015, *ApJ*, 802, L26
- Kacprzak, G. G., van de Voort, F., Glazebrook, K., et al. 2016, *ApJ*, 826, L11
- Kacprzak, G. G., Vander Vliet, J. R., Nielsen, N. M., et al. 2018, arXiv:1811.06028
- Kereš, D., Katz, N., Weinberg, D. H., & Davé, R. 2005, *MNRAS*, 363, 2
- Kewley, L. J., & Ellison, S. L. 2008, *ApJ*, 681, 1183
- Klypin, A. A., Trujillo-Gomez, S., & Primack, J. 2011, *ApJ*, 740, 102
- Kobayashi, C., & Nakasato, N. 2011, *ApJ*, 729, 16
- Kobulnicky, H. A., & Kewley, L. J. 2004, *ApJ*, 617, 240
- Kriss, G. A. 2011, *COS Instrument Science Report 2011-01(v1)*, 17 pages, 1
- Krogager, J.-K., Fynbo, J. P. U., Ledoux, C., et al. 2013, *MNRAS*, 433, 3091
- Lan, T.-W., Ménard, B., & Zhu, G. 2014, *ApJ*, 795, 31
- Lan, T.-W., & Mo, H. 2018, *ApJ*, 866, 36
- Lehner, N., Howk, J. C., Tripp, T. M., et al. 2013, *ApJ*, 770, 138
- Lehner, N., Wotta, C. B., Howk, J. C., et al. 2019, arXiv:1902.10147
- Lopez, S., Tejos, N., Ledoux, C., et al. 2018, *Nature*, 554, 493
- Mannucci, F., Cresci, G., Maiolino, R., et al. 2009, *MNRAS*, 398, 1915
- Martin, C. L., & Bouché, N. 2009, *ApJ*, 703, 1394
- Martin, C. L., Ho, S. H., Kacprzak, G. G., & Churchill, C. W. 2019, arXiv:1901.09123
- Martin, C. L., Shapley, A. E., Coil, A. L., et al. 2012, *ApJ*, 760, 127
- Ménard, B., & Fukugita, M. 2012, *ApJ*, 754, 116
- Moster, B. P., Somerville, R. S., Maulbetsch, C., et al. 2010, *ApJ*, 710, 903
- Murphy, M. T., Kacprzak, G. G., Savorgnan, G. A. D., & Carswell, R. F. 2019, *MNRAS*, 482, 3458
- Muzahid, S., Kacprzak, G. G., Charlton, J. C., & Churchill, C. W. 2016, *ApJ*, 823, 66
- Muzahid, S., Kacprzak, G. G., Churchill, C. W., et al. 2015, *ApJ*, 811, 132
- Nelson, D., Pillepich, A., Springel, V., et al. 2019, arXiv:1902.05554
- Ng, M., Nielsen, N. M., Kacprzak, G. G., et al. 2019, *ApJ*, submitted
- Nielsen, N. M., Churchill, C. W., Kacprzak, G. G., Murphy, M. T., & Evans, J. L. 2016, *ApJ*, 818, 171
- Nielsen, N. M., Churchill, C. W., Kacprzak, G. G., Murphy, M. T., & Evans, J. L. 2015, *ApJ*, 812, 83
- Nielsen, N. M., Kacprzak, G. G., Muzahid, S., et al. 2017, *ApJ*, 834, 148
- Nestor, D. B., Johnson, B. D., Wild, V., et al. 2011, *MNRAS*, 412, 1559
- Noterdaeme, P., Laursen, P., Petitjean, P., et al. 2012, *A&A*, 540, A63
- Noterdaeme, P., Srianand, R., & Mohan, V. 2010, *MNRAS*, 403, 906
- Oppenheimer, B. D., & Davé, R. 2009, *MNRAS*, 395, 1875
- Oppenheimer, B. D., Davé, R., Kereš, D., et al. 2010, *MNRAS*, 406, 2325
- Oppenheimer, B. D., Davé, R., Katz, N., et al. 2012, *MNRAS*, 420, 829
- Papovich, C., Labbé, I., Quadri, R., et al. 2015, *ApJ*, 803, 26
- Peeples, M. S., Corlies, L., Tumlinson, J., et al. 2018, arXiv:1810.06566
- Péroux, C., Bouché, N., Kulkarni, V. P., & York, D. G. 2013, *MNRAS*, 436, 2650
- Péroux, C., Bouché, N., Kulkarni, V. P., York, D. G., & Vladilo, G. 2011, *MNRAS*, 410, 2237
- Péroux, C., Quiert, S., Rahmani, H., et al. 2016, *MNRAS*, 457, 903
- Pettini, M., & Pagel, B. E. J. 2004, *MNRAS*, 348, L59
- Pilkington, K., Few, C. G., Gibson, B. K., et al. 2012, *A&A*, 540, A56
- Pointon, S. K., Kacprzak, G. G., Nielsen, N. M., et al. 2019, *ApJ*, submitted
- Pointon, S. K., Kacprzak, G. G., Nielsen, N. M., et al. 2019, *ApJ*, submitted
- Pointon, S. K., Nielsen, N. M., Kacprzak, G. G., et al. 2017, *ApJ*, 844, 23
- Prochaska, J. X., Weiner, B., Chen, H.-W., Mulchaey, J., & Cooksey, K. 2011, *ApJ*, 740, 91
- Prochaska, J. X., Werk, J. K., Worseck, G., et al. 2017, *ApJ*, 837, 169
- Prochter, G. E., Prochaska, J. X., O'Meara, J. M., et al. 2010, *ApJ*, 708, 1221
- Rahmati, A., & Oppenheimer, B. D. 2018, *MNRAS*, 476, 4865
- Ribaldo, J., Lehner, N., Howk, J. C., et al. 2011, *ApJ*, 743, 207
- Rosenwasser, B., Muzahid, S., Charlton, J. C., et al. 2018, *MNRAS*, 476, 2258
- Rubin, K. H. R., Prochaska, J. X., Koo, D. C., et al. 2014, *ApJ*, 794, 156
- Rubin, K. H. R., Prochaska, J. X., Koo, D. C., Phillips, A. C., & Weiner, B. J. 2010, *ApJ*, 712, 574
- Sánchez-Menguiano, L., Sánchez, S. F., Pérez, I., et al. 2018, *A&A*, 609, A119
- Sanders, R. L., Shapley, A. E., Kriek, M., et al. 2014, arXiv:1408.2521
- Schroetter, I., Bouché, N., Wendt, M., et al. 2016, *ApJ*, 833, 39
- Schroetter, I., Bouché, N. F., Zabl, J., et al. 2019, arXiv:1907.09967
- Sheinis, A. I., Bolte, M., Epps, H. W., Kibrick, R. L., Miller, J. S., Radovan, M. V., Bigelow, B. C., & Sutlin, B. M. 2002, *PASP*, 114, 851
- Shen, S., Madau, P., Guedes, J., et al. 2013, *ApJ*, 765, 89
- Simard, L., Willmer, C. N. A., Vogt, N. P., Sarajedini, V. L., Phillips, A. C., Weiner, B. J., Koo, D. C., Im, M., Illingworth, G. D., & Faber, S. M. 2002, *ApJS*, 142, 1
- Steidel, C. C., Kollmeier, J. A., Shapley, A. E., Churchill, C. W., Dickinson, M., & Pettini, M. 2002, *ApJ*, 570, 526
- Steidel, C. C., Rudie, G. C., Strom, A. L., et al. 2014, *ApJ*, 795, 165
- Stewart, K. R. 2011, arXiv:1109.3207
- Stocke, J. T., Keeney, B. A., Danforth, C. W., et al. 2013, *ApJ*, 763, 148
- Thom, C., Werk, J. K., Tumlinson, J., et al. 2011, *ApJ*, 736, 1
- Tremonti, C. A., Heckman, T. M., Kauffmann, G., et al. 2004, *ApJ*, 613, 898
- Tremonti, C. A., Moustakas, J., & Diamond-Stanic, A. M. 2007, *ApJ*, 663, L77
- Tripp, T. M., Jenkins, E. B., Bowen, D. V., et al. 2005, *ApJ*, 619, 714
- Tripp, T. M., Meiring, J. D., Prochaska, J. X., et al. 2011, *Science*, 334, 952
- Tumlinson, J., Peeples, M. S., & Werk, J. K. 2017, *ARA&A*, 55, 389
- Tumlinson, J., Thom, C., Werk, J. K., et al. 2013, *ApJ*, 777, 59
- van de Voort, F., & Schaye, J. 2012, *MNRAS*, 423, 2991
- van Dokkum, P. G. 2001, *PASP*, 113, 1420
- Veilleux, S., Cecil, G., & Bland-Hawthorn, J. 2005, *ARA&A*, 43, 769
- Weiner, B. J., et al. 2009, *ApJ*, 692, 187
- Werk, J. K., Prochaska, J. X., Thom, C., et al. 2012, *ApJS*, 198, 3
- Werk, J. K., Prochaska, J. X., Thom, C., et al. 2013, *ApJS*, 204, 17
- Werk, J. K., Prochaska, J. X., Tumlinson, J., et al. 2014, *ApJ*, 792, 8
- Wotta, C. B., Lehner, N., Howk, J. C., et al. 2019, *ApJ*, 872, 81
- Wotta, C. B., Lehner, N., Howk, J. C., O'Meara, J. M., & Prochaska, J. X. 2016, *ApJ*, 831, 95
- Wuyts, E., Wisnioski, E., Fossati, M., et al. 2016, *ApJ*, 827, 74
- Zabl, J., Bouché, N. F., Schroetter, I., et al. 2019, *MNRAS*, 485, 1961
- Zahedy, F. S., Chen, H.-W., Johnson, S. D., et al. 2019, *MNRAS*, 484, 2257
- Zahid, H. J., Dima, G. I., Kudritzki, R.-P., et al. 2014, *ApJ*, 791, 130